Materials Research Proceedings 41 (2024) 1472-1481 https://doi.org/10.21741/9781644903131-163

Study on the numerical prediction quality of material models regarding springback of hollow embossed metallic bipolar half-plates

BECK Maxim[1,a*], KARADOGAN Celalettin[1], CYRON Patrick[1], ROUVEN RIEDMÜLLER Kim[1] and LIEWALD Mathias[1]

[1]Institute for Metal Forming Technology, University of Stuttgart, Holzgartenstr. 17, 70174 Stuttgart, Germany

[a]maxim.beck@ifu.uni-stuttgart.de

Keywords: Bipolar Plate, Springback Prediction, Forming Simulation

Abstract. Due to the ongoing endeavors to reduce CO_2 emissions in the energy sector, particularly through advancements in electric mobility, the demand for thin metallic components is currently increasing. This demand is notably apparent for bipolar plates, which are used in fuel cells. The production of these bipolar plates requires high-precision hollow embossing of thin metallic foils with thicknesses below 100 µm. Even minor variations in this process can result in forming defects and undesirable springback in produced parts. A robust design of manufacturing processes for bipolar plates therefore necessitates the implementation of accurate finite element analysis (FEA), since this is crucial for predicting material behavior during and after the forming process. However, the precision of such simulations is heavily dependent on the material models employed. For this reason, the study presented in this paper specifically focused on the numerical modeling of high-precision hollow embossing of bipolar half-plates. For this purpose, a comprehensive material characterization of a 1.4404 stainless-steel foil with a thickness of 0.1 mm was conducted first. Moreover, an experimental laboratory geometry and a corresponding laboratory tool for the hollow embossing of miniaturized bipolar half-plates was developed in order to enable a comprehensive evaluation of the simulation results. The validation and assessment of widely used material models for metal forming in LS-Dyna, exemplified by MAT_036 Barlat '89 and MAT_133 Barlat 2000, were effectively demonstrated through experimental forming tests. These tests confirmed distinct performance differences between the two material models concerning springback and thinning. Importantly, it was confirmed that the simpler MAT_036 model exhibits high accuracy in predicting both springback and thinning, emphasizing its effectiveness in capturing relevant deformation properties during the hollow embossing process.

Introduction

Efficient and environmentally sustainable powertrain systems are essential for advancing the environment friendly electrification of both passenger and commercial transportation. In this context, fuel cell technology is emerging as a compelling alternative to conventional electrical drives, particularly for heavy-duty and long-distance applications. The accompanying rise in demand for fuel cell systems has led to a notable increase in the production volume of metallic bipolar plates made of thin stainless-steel foils having thicknesses below 100 µm. However, the manufacturing of such high-precision metallic bipolar plates using processes such as hollow embossing is significantly challenging. Foils with thicknesses of around 100 µm and less are prone to defects such as microcracks, cracks and wrinkles and are difficult to handle during production [1-4]. In addition, the phenomenon of springback still remains a major issue in achieving dimensional accuracy of components made from thin metallic foils [1, 5-6]. Flow channels as well as the overall geometry must meet very precise dimensional tolerances of a couple micrometers in both vertical and lateral directions [1, 7]. Otherwise, problems may arise during the subsequent joining of the bipolar half-plates, which can lead to misalignment issues affecting the performance

Materials Research Proceedings 41 (2024) 1472-1481 https://doi.org/10.21741/9781644903131-163

and efficiency of the entire fuel cell stack. These limitations result in extended production cycle times and increased costs for quality assurance, hindering the economical manufacturing of high quantities of bipolar half-plates until this day [1].

To address these challenges and to optimize forming processes of bipolar half-plates at an early stage of development, nowadays finite element simulations are essential. However, the accuracy of these simulations, which is crucial for obtaining virtual results of complex forming processes, heavily relies on the accurate modeling of material behavior and thus the material characterization procedures [1, 8].

The study presented in this paper aims to evaluate the widely used material models *"MAT_3-PARAMETER_BARLAT"* (MAT_36) and *"MAT_BARLAT YLD2000"* (MAT_133) in LS-Dyna regarding the prediction accuracy for hollow-embossed bipolar half-plates made of 1.4404 stainless-steel foil (t_0 = 100 µm). For this purpose, an in-depth material characterization was conducted through tensile and bulge tests, enabling comprehensive material modeling of the stainless-steel used. Building upon the findings of previous studies [1], a suitable laboratory-scale prototype tool was developed, demonstreating key features of an actual bipolar half-plate. This tool made the comprehensive comparison between simulation results and real experiments possible. Here, the thickness distribution within the channels, the overall flatness and the springback behavior of the manufactured part were precisely measured and compared with the FE-model.

Modeling and numerical study

Material characterization and modeling.

In the present study, the austenitic stainless-steel 1.4404 with a thickness of t_0 = 100 µm was used as test material. This material is frequently used today for the manufacturing of metallic bipolar plates. For determining required material parameters, quasi-static uni-axial tensile tests according to DIN EN 6892 were carried out on specimen according to DIN 50125 Form H 20 x 80 prepared in 0°, 45° and in 90° rolling directions. Additionally, bulge tests according to ISO 16808 were performed to obtain experimental data for higher true strain values as well as for the biaxial yield stress. For r_b, a value of 1.0 was chosen according to [9]. For both characterization tests optical measurements and strain evaluation were performed using a GOM ARAMIS system. The material parameters given in Table 1 were obtained by averaging the results of three repetitions in each case as explained in the next paragraph.

Table 1: Material properties of stainless-steel 1.4404, t_0 = 100 µm.

σ_0 [MPa]	σ_{45} [MPa]	σ_{90} [MPa]	σ_b [MPa]	r_0 [-]	r_{45} [-]	r_{90} [-]	r_b [-]
243.45	250.89	253.51	228.42	0.72	1.06	1.22	1.0

Corresponding averaged true-stress – true-strain curves obtained by tensile and bulge tests are depicted in Fig. 1. Here, the true-stress – true-plastic-strain curve is shown for the rolling direction tensile test as well as for the bulge test. Averaged true-stress – true-strain curves for rolling directions of 45° and 90° were also used to obtain the anisotropy ratios (σ_{45}/σ_{00}, σ_{90}/σ_{00}, σ_B/σ_{00}) on the initial yield-locus based on the principle of plastic-energy equivalency.

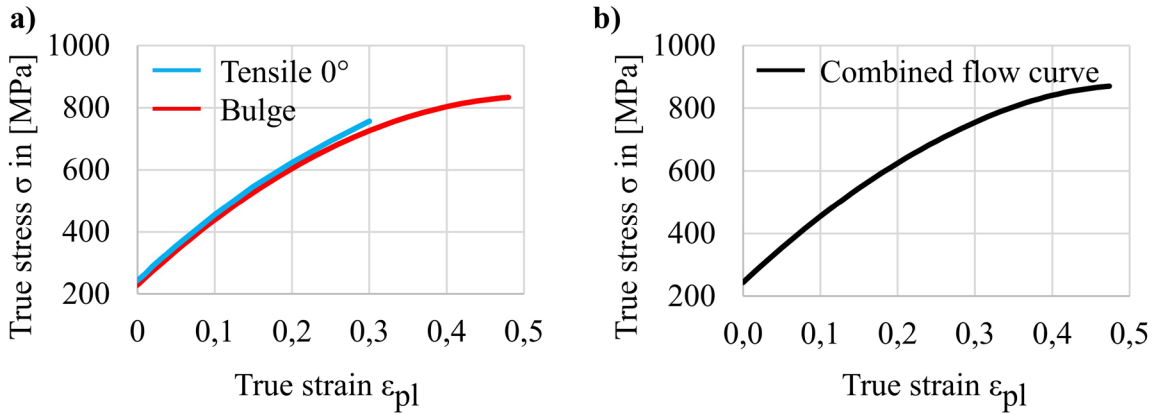

Fig. 1: (a) True stress - true strain curves obtained by tensile and bulge tests and (b) combined flow curve.

Using the obtained anisotropy ratio for the bulge test, the true-stress – true-plastic-strain diagram of the bulge test was used to obtain an experimental extension for the flow curve using the equivalent plastic deformation energy approach as described in [10]. Finally, a suitable flow curve is obtained, as shown in Fig. 1 b). The final flow curve for use in forming simulations is approximated by the Hockett-Sherby formula according to [11], see Eq. 1.

$$\sigma_{Hockett-Sherby} = \sigma_{Sat} - (\sigma_{sat} - \sigma_{ini}) \cdot e^{-a \cdot \varepsilon_{pl}^{p}} \quad (1)$$

Table 2: Parameters describing the flow-curve approximation according to Hockett-Sherby.

σ_{sat} [MPa]	σ_{ini} [MPa]	p [-]	a [-]
993.43	243.45	1.12	4.397

In the LS-Dyna software package, these acquired material data was adopted for the material model MAT_036 - *"MAT_3-PARAMETER_BARLAT"* by following the methodology outlined in [13], and for MAT_133 - *"MAT_BARLAT YLD2000"* according to [9]. The characteristic parameters were entered through the corresponding input interfaces in LS-Dyna.

Laboratory bipolar half-plate geometry and experimental setup.
Based on common designs and preliminary studies regarding the formability of bipolar plate geometries, a laboratory bipolar half-plate geometry was developed [1]. The design is shown in Fig. 2 which has an active surface area of 84 mm x 50 mm and incorporates key features of bipolar plates such as a flow field, inlet and outlet ports for gaseous media as well as a surrounding sealing bead. This geometry does not possess any specific functional characteristics relevant to the fuel cell, but primarily serves to validate forming simulations and material models and to gain a more comprehensive understanding of the manufacturing process.

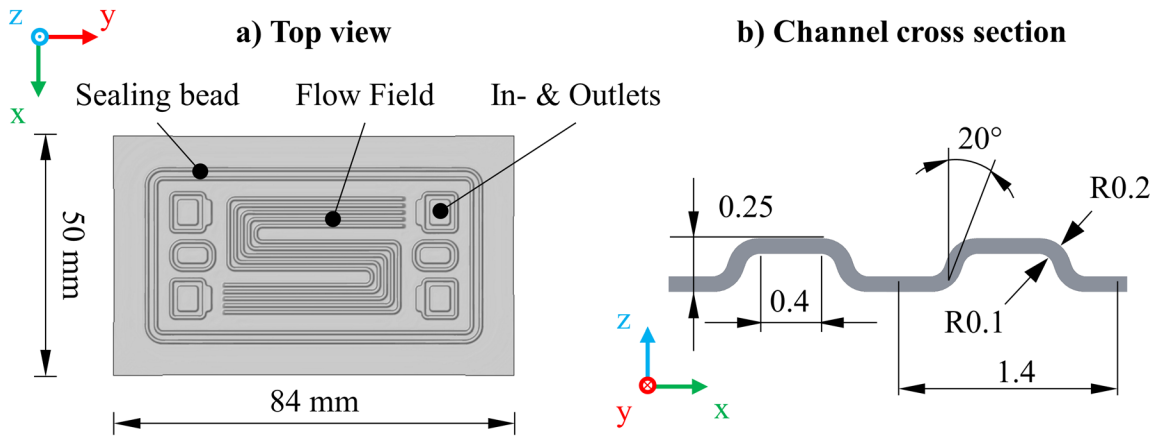

Fig. 2: (a) Top view of developed laboratory geometry showing characteristics of a metallic bipolar half-plate and (b) the designed channel cross section of the bipolar half-plate.

To produce the laboratory specimen shown above, a tool-set for conventional hollow embossing with a massive punch and a die was manufactured. The active surfaces of the upper and lower tool have been offset according to the given foil thickness of $t_0 = 0.1$ mm. Precise alignment of the tool inserts was ensured by appropriate manufacturing accuracy, adherence to tolerance specifications and the incorporation of guiding columns into the tool. No blank holder was used in the laboratory-scale investigations presented here. The configuration of the laboratory tool and its installation in the hydraulic press having a maximum press force of 1600 kN is shown in Fig. 3. A load cell and displacement sensor have been added to the tool frame to measure punch force and stroke.

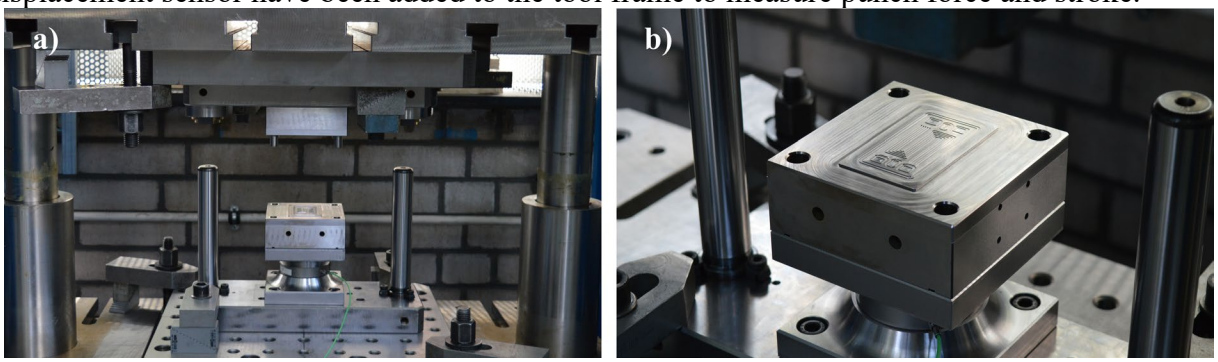

Fig. 3: (a) Laboratory tool in the press and (b) detailed view of the active tool surface of lower die.

In order to determine the minimum embossing force required for the shown laboratory geometry of a bipolar half-plate, an initial experimental test-series was conducted with variable punch forces. Subsequently, the achieved embossing depth was measured through optical measurements of the flow field geometry using a GOM ATOS system. Here, it was found that at a press force of 120 kN, the embossing depth of 0.25 mm and thus complete forming of the specimen could be achieved. The corresponding optical measurements of the embossed channels and their depths are presented in the following Fig. 4. For simplicity, only sections of the specimen have been considered, and average local depth of channels was evaluated. In this localized analysis, any springback effects have been neglected.

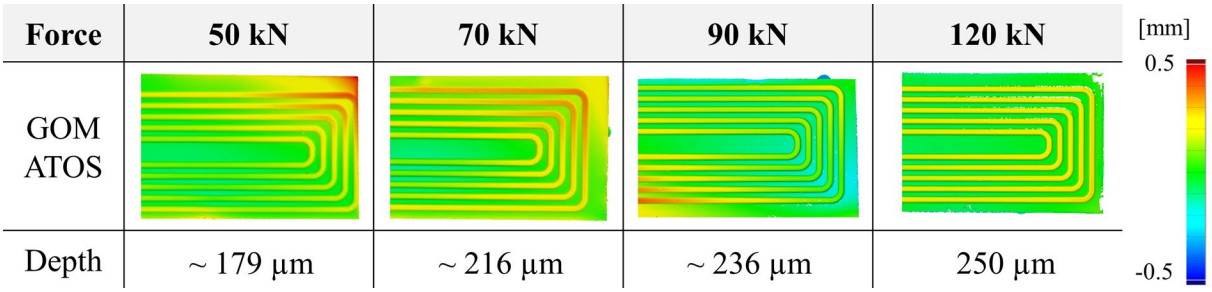

Fig. 4: Comparison of embossing force and embossing depth. Measurements obtained by GOM ATOS.

According to these results, the bipolar half-plates that were produced in further tests were embossed with a constant press force of F_{max} = 120 kN, ensuring comparability of the results. Moreover, no additional lubrication was applied and only the lubricant present on the supplied foils was used during the forming operations.

FE model setup.

Based on the previously introduced laboratory geometry, forming simulations of the hollow embossing process were set up. These simulations aimed to evaluate the simulation accuracy in relation to the real experiments and to assess the performance of the material models considered. For the forming simulations, the LS-Dyna software package with solver version R12.1 was used. The model, consistent with real experiments, consisted of a blank with size of 84 mm x 50 mm and was meshed with fully integrated shell elements of type "-16" with seven integration points in thickness direction. A constant mesh size of 0.025 mm (edge-length) was applied, allowing the fine radii in the geometry (see Fig. 2 and Fig. 5) to be adequately represented. This meshing strategy resulted in a total of 6.72 million elements in the metallic foil for simulating the hollow embossing process. Due to the fine meshing, distortions of the mesh during the forming process could also be prevented (see Fig. 5).

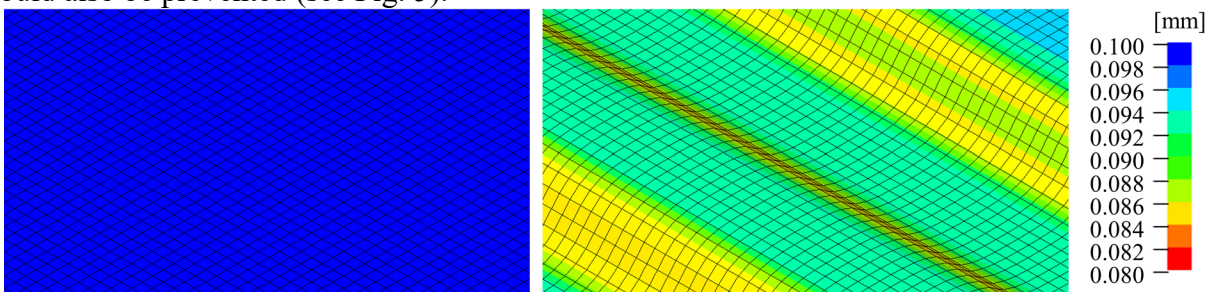

Fig. 5: Detailed mesh view with thickness distribution: a) Before and b) after hollow embossing.

The active tool surfaces were meshed more finely with element sizes ranging from 0.01 mm to 0.025 mm. The die was fixed, as in the real process, while the punch was allowed to move vertically corresponding to the real process. For the simulation, a conservative friction coefficient of $\mu = 0.20$ was set in a coulomb friction model based on empirical values from previous studies.

The parameters for mass scaling and contact definition were refined through numerical investigations to optimize computational efficiency without significantly changing the forming simulation results. This way a mass scaling of -2.0 e-07 and "FORMING_SURFACE_TO_SURFACE" contact formulation was used. The final configuration resulted in a computation time of approximately 12 hours using the explicit solver, 32 Intel® Xeon® Gold 6230 cores at 2.10 GHz and approximately 50 Gigabyte of RAM. The calculation of the resulting springback based on the results gained from the forming simulation and required approximately two hours when using an implicit solver. Further details on the boundary conditions

of the springback simulation are provided in the subsequent chapter entitled "Results and discussion".

Results and discussion

The forming simulations were conducted using the material models MAT_036 and MAT_133 based on the material properties outlined above. For the comparison between simulation and reality, both the thickness distributions within the active flow field geometry as well as the global springback of the entire bipolar half-plate geometry were analyzed. For comparison purposes, statistically averaged component data from real measurements was used.

Analysis of the thickness distribution.

The thickness distributions obtained for the two material models from the forming simulations are illustrated in Fig. 6. It is evident that material thinning primarily concentrates on the flow field geometry within the inner region of the bipolar half-plate.

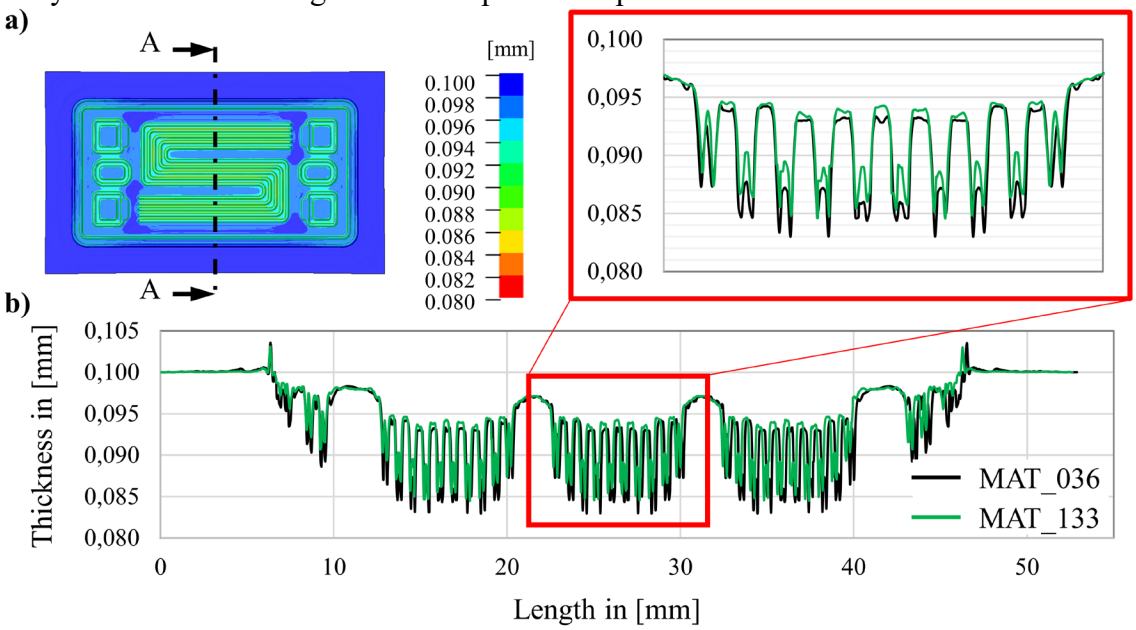

Fig. 6: (a) Top view of formed specimen. (b) Thickness distribution in the forming simulation by utilizing MAT_036 and MAT_133 – exemplary comparison along the mid-cross-section A-A.

The average material thinning ranges from approximately 5 to 15% showing individual peaks in areas of flow field direction changes. The maximum thinning was calculated higher at 19.16% when using the material model MAT_036 than with the material model MAT_133, which is limited to 16.37%. When examining the mid-cross-section A – A (see Fig. 6), it becomes clear that significant differences in material thinning can be observed, particularly in the flow field. Such differences are explained in more detail in the analysis of Fig. 7.

For the analysis of the resulting thickness distributions in the real component, the embossed laboratory bipolar half-plates were cut and cross-sections were prepared according to the cutting plane A – A in Fig. 6. In this way, the remaining material thickness after forming could be measured using a microscope and be compared with results from the forming simulation. This publication focuses on the comparison of only a few exemplary channels and not all of the 19 in total due to similar conditions in the respective hollow embossed channels. The corresponding cross-sectional analysis for channels 2, 3, 8 and 10 can be seen in Fig. 7. Seven distinct measurement positions were established for each channel, with four thickness measurements in the radii area and three thickness measurements in the region of flat channel bottoms and channel

Materials Research Proceedings 41 (2024) 1472-1481 https://doi.org/10.21741/9781644903131-163

sidewalls. In line with previous investigations, the mean value from three measurements were used for statistical robustness.

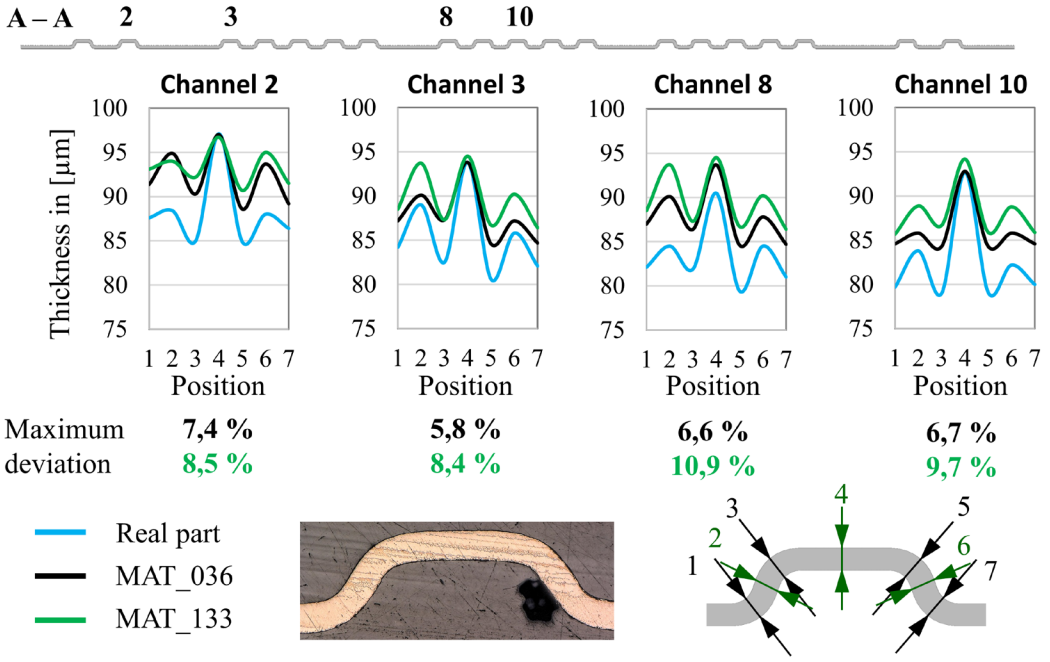

Fig. 7: Distribution of foil thickness at selected channel cross-sections – Real part measurement (blue), simulation with MAT_036 (black) and simulation with MAT_133 (green).

In addition to the real component data (in blue), the simulation results, which correspond to the color scheme from previous Fig.s, are also presented. Here, a maximum thinning can be observed at the measurement positions of the radii, while a greater material thickness is detected in the flat areas of the channel bottom and sidewall. The foil thickness generally decreases from the outer regions in the geometry (Channel 2) towards the center of the component (Channel 10) due to restricted material flow. While outer channels support relative motion of foil in the die leading to higher foil thicknesses, inner channels exhibit lower thicknesses. Here, the material flows out of thickness due to high tension stresses, as expected. As a result, both material models can qualitatively represent the foil thickness distribution within the channels, with higher absolute deviations observed at the measurement positions of the radii. Generally, material model MAT_036 shows lower deviation in the investigations, although the simulation results are less critical than reality. This could possibly be attributed to the limited capability of shell elements to represent changes in foil thickness in thickness direction.

Analysis of springback behavior.

Springback refers to the geometric alteration that occurs to a component after it is freed from the forming tool's forces at the end of a forming process. To numerically determine the resulting springback, the results of the forming simulation were transferred to a separate simulation. In this process, the occurring strains and stresses of the respective elements were exported in a separate restart-file also known as a „.dynain file". In a subsequent step, the resulting springback was determined using an implicit calculation in LS-Dyna. Boundary conditions for the springback simulation were chosen accordingly to the springback measurements in reality. The bipolar half-plate was fixed in a defined state using clay, allowing for a comparison between real data and simulation (see Fig. 8). In the simulation, the corresponding degrees of freedom at the corners of

the plate were constrained. Thus, the occurrence of unstable springback conditions could be prevented. Real component measurements were conducted using GOM ATOS as shown in Fig. 8.

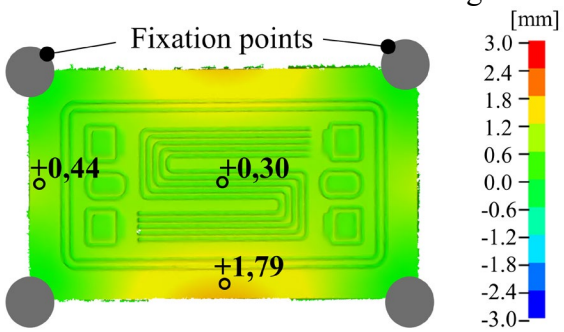

Fig. 8: Springback of the laboratory bipolar half-plate when clamped at four corners (real part) measured with GOM ATOS.

During the investigations, it was observed that all real components exhibited nearly consistent springback behavior in each experimental repetition. Thus, only one bipolar half-plate is considered in the following Fig. 9 for an exemplary analysis. Finally, it can be observed that especially the flange areas exhibit a significant amount of springback, whereas the flow field region shows relatively lower levels of springback in proportion. Similar effects were observed during the simulations. Both material models MAT_036 and MAT_133 were able to represent the springback behavior, with MAT_036 showing a very good match, especially when considering the absolute values of the resulting springback (refer to Fig. 9).

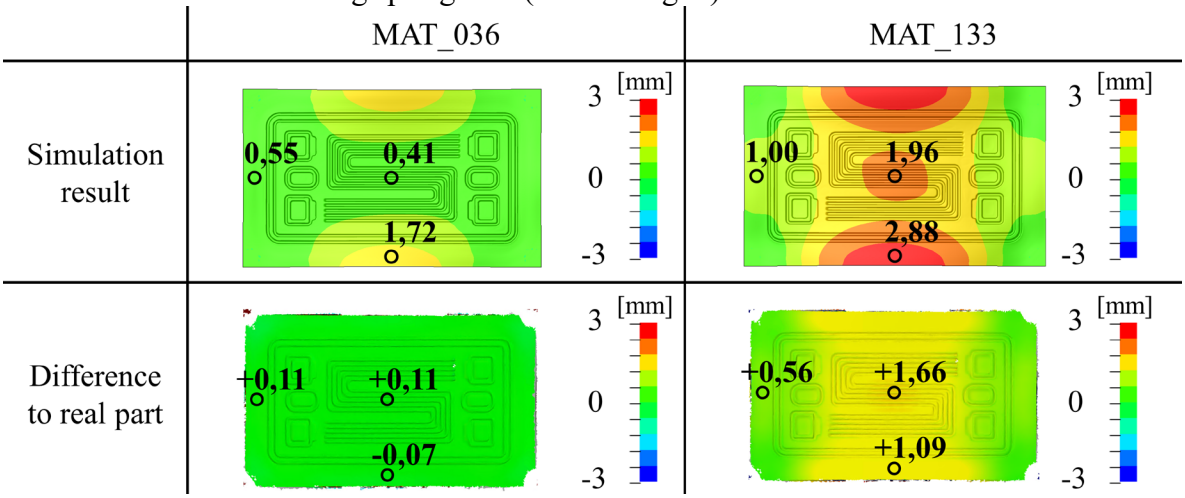

Fig. 9: Comparison of springback simulation results with real component data.

The use of MAT_133 leads to an overestimation of the actual springback under otherwise constant boundary conditions. These discrepancies arise from the variation in deformation due to different material modeling approaches, as already highlighted in Fig. 6 and Fig. 7.

Summary and Outlook

The study as presented in this paper investigated the potential of LS-Dyna-based shell models and widely used material models *"MAT 3-PARAMETER BARLAT"* (MAT_036) and *"MAT_BARLAT YLD2000"* (MAT_133) regarding the accurate prediction of the quality of hollow-embossed bipolar half-plates made of 1.4404 stainless-steel foil. For this an extensive material characterization was conducted previously and a corresponding laboratory-scale prototype tool for hollow embossing of bipolar half-plates was developed. Based on the preceding investigations using simulation results and real part data, the following can be concluded:

- The distribution of thinning can be predicted in forming simulations with LS-Dyna with minimal deviations. Notable differences arise in the material models, particularly in the areas of radii, with MAT_036 demonstrating better predictive accuracy and a lower relative deviation of max. 7.4 %. Whereas the maximum deviation with MAT_133 is max. 10.9 %.
- The springback can be reliably predicted. Particularly, the material model MAT_36 can reproduce the absolute values with high precision - almost no significant differences in the presented hollow embossing process are notable with deviation between -0.07 mm and +0.11 mm. However, MAT_133 exhibits significant deviations in this aspect, with values between +1.00 mm and +2.88 mm compared to measured real part data.
- Reliable prediction of the resulting quality of hollow embossed bipolar half-plates using common material models in LS-Dyna is possible, although there is further potential for improvement in the accuracy of thickness distribution predictions, requiring additional modeling effort. This can possibly be achieved through more complex shell element formulations.

This comparative analysis has offered valuable insights into the achievable predictive accuracy of the considered common material models in LS-Dyna, thereby enhancing the efficiency of future design processes. Subsequent studies will particularly focus on multi-stage hollow-embossing processes, commonly employed in the production of larger bipolar half-plates. In addition to the simple material models presented here, more intricate material models will be employed. These models can account for kinematic hardening and the Bauschinger effect resulting from cyclic loading and unloading between multiple forming stages. Relevant foundations and approaches have already been introduced in [13].

Acknowledgements
This work was supported within the “DFG-Fraunhofer Transfer Programme”, established by the German Research Foundation (DFG-Project 460294948). Authors feel grateful for the financial support. In addition, the authors would like to thank the Working Group Foil-Forming established at the Institute for Metal Forming Technology, University of Stuttgart for their support.

References

[1] M. Beck, K. R. Riedmüller, M. Liewald, A. Bertz, M. J. Aslan, D. Carl, Investigation on the influence of geometric parameters on the dimensional accuracy of high-precision embossed metallic bipolar plates, Production at the Leading Edge of Technology WGP (2022) 427-438. http://dx.doi.org/10.1007/978-3-031-18318-8_44

[2] F. Vollertsen, D. Biermann, H. N. Hansen, I.S. Jawahir, K. Kuzman, Size effects in manufacturing of metallic components, CIRP Ann Manuf Technol 58 (2009) 566-587. https://doi.org/10.1016/j.cirp.2009.09.002

[3] D. M. Neto, M. C. Oliveira, J. L. Alves, L. F. Menezes, Numerical study on the formability of metallic bipolar plates for proton exchange membrane (PEM) fuel cells, Metals 9 (2019) 810. https://doi.org/10.3390/met9070810

[4] Q. Hu, D. Zhang, H. Fu, K. Huang, Investigation of stamping process of metallic bipolar plates in PEM fuel cell – numerical simulation and experiments, Int. J. Hydrogen Energy 39 (2014) 13770-13776. http://dx.doi.org/10.1016/j.ijhydene.2014.01.201

[5] A. Bauer, Experimentelle und numerische Untersuchungen zur Analyse der umform-technischen Herstellung metallischer Bipolarplatten, Dissertation, Technische Universität Chemnitz, Chemnitz, 2020.

[6] F. Adzima, T. Balan, P. Y. Manach, Springback prediction for a mechanical micro connector using CPFEM based numerical simulations, Int J Mater Form 13 (2020) 649-659. https://doi.org/10.1007/s12289-019-01503-5

[7] S. Porstmann, T. Wannemacher, W. G. Drossel, A comprehensive comparison of state-of-the-art manufacturing methods for fuel cell bipolar plates including anticipated future industry trends, J Manuf Process 60, 366-383. https://doi.org/10.1016/j.jmapro.2020.10.041

[8] C. Pham, F. Adzima, J. Coër, Anti-buckling device for ultra-thin metallic sheets under large and reversed shear strain paths, Experimental Mechanics 57, 593-602. https://doi.org/10.1007/s11340-017-0256-4

[9] F. Barlat, J. C. Brem, J. W. Yoon, K. Chung, R. E. Dick, D. J. Lege, et al., Plane stress yield function for aluminum alloy sheets – part 1: theory, International Journal of Plasticity 19(9) (2003) 1297-1319. https://doi.org/10.1016/S0749-6419(02)00019-0

[10] A. Mutrux, B. Hochholdinger, P. Hora, A procedure for the evaluation and validation of the hydraulic biaxial experiment, Numisheet (2008).

[11] J. E. Hockett, O. D. Sherby, Large strain deformation of polycrystalline metals at low homologous temperatures, J Mech Phys Solids 23 (1975) 87–98. https://doi.org/10.1016/0022-5096(75)90018-6

[12] F. Barlat, K. Lian, Plastic behavior and stretchability of sheet metals. Part 1: A yield function for orthotropic sheets under plane stress conditions, International Journal of Plasticity 5(1) (1989) 51-66. https://doi.org/10.1016/0749-6419(89)90019-3

[13] C. Karadogan, M. Beck, P. Cyron, K. R. Riedmüller, M. Liewald, Development of a new cyclic shear test setup for characterizing thin metallic foils, IOP Conference Series Materials Science and Engineering (2023), http://dx.doi.org/10.1088/1757-899X/1284/1/012057